CFD AND EXPERIMENTAL ANALYSIS OF SINGLE PHASE BUOYANCY DRIVEN COUNTER-CURRENT FLOW IN A PIPE

F. Sebilleau, R. I. Issa, and S. P. Walker
Department of Mechanical Engineering
Imperial College London
Exhibition Road, London UK SW7 2AZ
frederic.sebilleau11@imperial.ac.uk; r.issa@imperial.ac.uk; s.p.walker@imperial.ac.uk

A. Kansal, N. K. Maheshwari
Bhabha Atomic Research Center (BARC)
Mumbai, India
akansal@barc.gov.in; nmahesh@barc.gov.in

1. ABSTRACT

In the present paper, we study single-phase counter-current flow in a circular pipe as a model problem that is representative of flows occurring under various circumstances in a reactor primary loop, for example when emergency-cooling (ECCS) water is injected in the hot leg or when cooler fluid flows from the steam generator in the hot leg. In order to isolate the complexity of the turbulent mixing generated by buoyancy driven single-phase counter current flow, an experimental rig was built at the Bhabha Atomic Research Center (BARC) to validate CFD model predictions. This new rig is composed of two tanks of water linked by an inclined circular pipe. Initially the upper tank is filled with cold water and the lower one with heated water and the different-density fluids are allowed to mix under the influence of gravity.

In this paper, thermocouple measurements of temperature at several locations in the rig are presented for several temperature differences and tilt angles. These experimental measurements are compared with state of the art highly-resolved large eddy simulation (LES). These LES computations (carried out with the commercial CFD package STAR-CCM+) give detailed information on the behaviour of the turbulence in such flow as well as serve to assess the performance of some uRANS two-equation eddy viscosity models that are also tested.

2. KEYWORDS
Single Phase counter-current flow/ Buoyancy/ CFD/ LES/ uRANS

1. INTRODUCTION

New nuclear reactor concepts tend to rely as much as possible on passive cooling systems. At the same time, the advances in computational resources made CFD a desirable tool to aid the design of new reactors. However, the industry standard turbulence models were initially developed using some asymptotic characteristics of isotropic turbulence at very high Reynolds number. Therefore the applicability and accuracy of the predictions of such models for buoyancy driven flows, which have a particularly low level of turbulence, is not obvious and requires experimental validation. This is the purpose of present paper.

In the present work, we focus on the analysis of the capabilities of several commonly used uRANS turbulence models to predict single-phase buoyancy driven counter-current flow in a pipe. These flows arise when an unstable density gradient induces turbulent mixing in a wall-bounded geometry such as a

pipe. The physics of this type of flow also occurs in different configurations in a reactor primary loop. For instance, when a body of cold fluid flows downwards from the steam generator to the reactor core via the hot leg or when cold water is injected in accidents circumstances [1] or even with a passive ECCS system. In order to ensure the reliability of natural circulation processes, the influence of such counter-current flows needs to be understood and predicted accurately. The most important aspect sought from the CFD analysis is to identify reliable techniques for the accurate prediction of the velocity field, which ultimately determines the flow rates in the primary circuit; the latter is the most important element in predicting the reliability or potential weakness of a particular passive system to maintain the core safe under accident scenarios. In the present paper, a simple configuration giving rise to buoyancy driven mixing in a straight circular pipe is considered.

Analysis of such flows in the literature can only be found in recent publications and those focused on the qualitative study of the phenomena. Examples of such investigations can be found in [2-5]. To the authors' knowledge, the only CFD analysis of such flow configuration using classic uRANS model is given in our previous work [6], where accurate PIV measurements given in [4] were used for comparison. That study considered the turbulent mixing in a long slender pipe inclined at 15deg from vertical where pure water and water + $CaCl_2$ were initially placed respectively in the lower and upper parts of the pipe. No other accurate quantitative measurements were found in the literature to extend the CFD analysis carried out for a wider range of parameters.

The purpose of the present paper is to provide additional experimental measurement as well as highly resolved LES results for the given configuration. An analysis of the prediction of several two-equations eddy viscosity turbulence models is then carried out and compared with LES and experimental results. The commercial CFD code STAR-CCM+ v9.04 [7] is used for all the simulations presented herein.

2. THE EXPERIMENTAL SETUP

2.1. Rig Design

The initial design of the experimental rig used in the present paper was presented in [8] and its CAD model is shown in Figure 1a. The rig is composed of two large water tanks linked by an acrylic pipe with a ball valve in central position. The tilt angle of the pipe can vary between 0 deg to 40 deg from the vertical. The length of the pipe section is 1.5m with an internal diameter of 40.9mm. The distance between the two tanks is 2.06m. Each tank has a diameter of 500mm and a length equal to 350mm. The rig was built at BARC (Bhabha Atomic Ressearch Center) under the Indo-UK collaboration program. With the ball valve closed the upper part is filled with water at room temperature whilst the lower part is filled with water heated by a 4kW electric heater to a prescribed temperature difference between the two tanks. In order to avoid the formation a thermal stratification before the beginning of the experiment, a recirculation pump is used to homogenize the temperature in the lower part of the rig. Once this procedure is complete, the ball valve is opened and the data acquisition system starts recording the data.

The advantage of the present new rig design over others in the existing literature on buoyancy-driven counter-current flow is the use of the two large water tanks. These have very large thermal inertia and therefore behave as almost constant sources of cold and hot water. This allows the flow in the pipe to attain a quasi statistically steady state, which is appropriate for CFD comparisons. More details will be given about the last point later in the paper.

2.2. Experimental Conditions

In the present paper, only one flow configuration is studied. The details of this configuration as well as the fluid properties are summarized in Table I.

Table I: Reference fluid properties and experiment configuration

Quantity	Symbol	Value
Cold tank temperature (K)	T_c	308
Hot tank temperature (K)	T_h	328
Tilt angle (deg)	θ	30
Reference Temperature (K)	T_{ref}	318
Reference pressure (Pa)	P_{ref}	10^5
Reference density (kg/m^3)	ρ_0	989.864
Dynamic viscosity (Pa-s)	μ	5.9765×10^{-4}
Specific heat (J/kg-K)	c_p	4180.1
Thermal conductivity (W/m-K)	k	0.63719
Thermal expansion coefficient (1/K)	β	4.26×10^{-4}

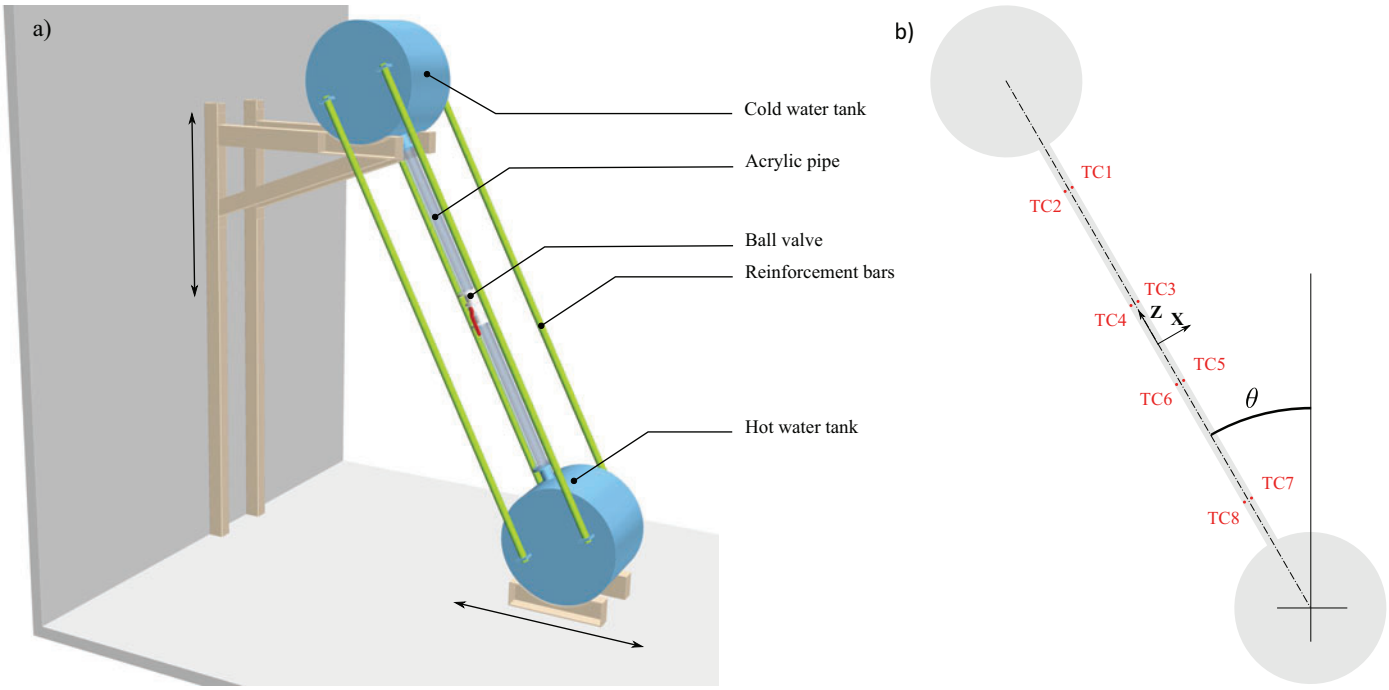

Figure 1: a) CAD model of the BARC rig b) Position of the origin of the coordinate system used in the present paper and approximate positions of the thermocouples.

2.3. Measurement Setup.

The present experimental setup uses only thermocouple measurements. The rig contains many thermocouples placed at various locations. The detailed position of each thermocouple is summarized in Table II below. The origin of the coordinate system used to define their position is located on the axis of the pipe, in the centre as illustrated in Figure 1b.

Type K thermocouple with a diameter of 0.5 mm are used. The acquisition system records the temperature every 50ms.

Table II: Exact position of the thermocouple shown in Figure 1b

Thermocouple	X (m)	Y (m)	Z (m)
TC1	0.00435	0.0	0.617
TC2	-0.00505	0.0	0.617
TC3	0.00456	0.0	0.153
TC4	-0.00609	0.0	0.153
TC5	0.00655	0.0	-0.153
TC6	-0.00576	0.0	-0.153
TC7	0.00619	0.0	-0.617
TC8	-0.00787	0.0	-0.617

3. CFD METHODOLOGY

3.1. CFD model

In the present paper, the general Navier-Stokes and the total energy equations are solved within a finite volume framework, using the fully unstructured commercial CFD package STAR-CCM+ v9.04 from CD-Adapco [7]. The computational domain is illustrated in Figure 2a. The dimensions of the computational domain closely follow the dimensions of the experimental rig given in section 2.1. All the surfaces shown in grey in Figure 2 are no-slip walls with adiabatic boundary condition for energy. In the experimental setup the temperature of the cold tank is equal to the ambient air temperature of the room so there is no heat loss in the upper section of the rig and the maximum temperature difference between the water inside the rig and the ambient air is 20K in the present case. A simple hand calculation can show than even in the worse case scenario where all the acrylic pipe is filled with water 20K above the ambient air temperature (which is far from being the case), the heat loss remains negligible (a few watts) as the thermal conductivity of acrylic is only around 0.2W/m/K and the convective heat transfer coefficient between acrylic and air is also very small.

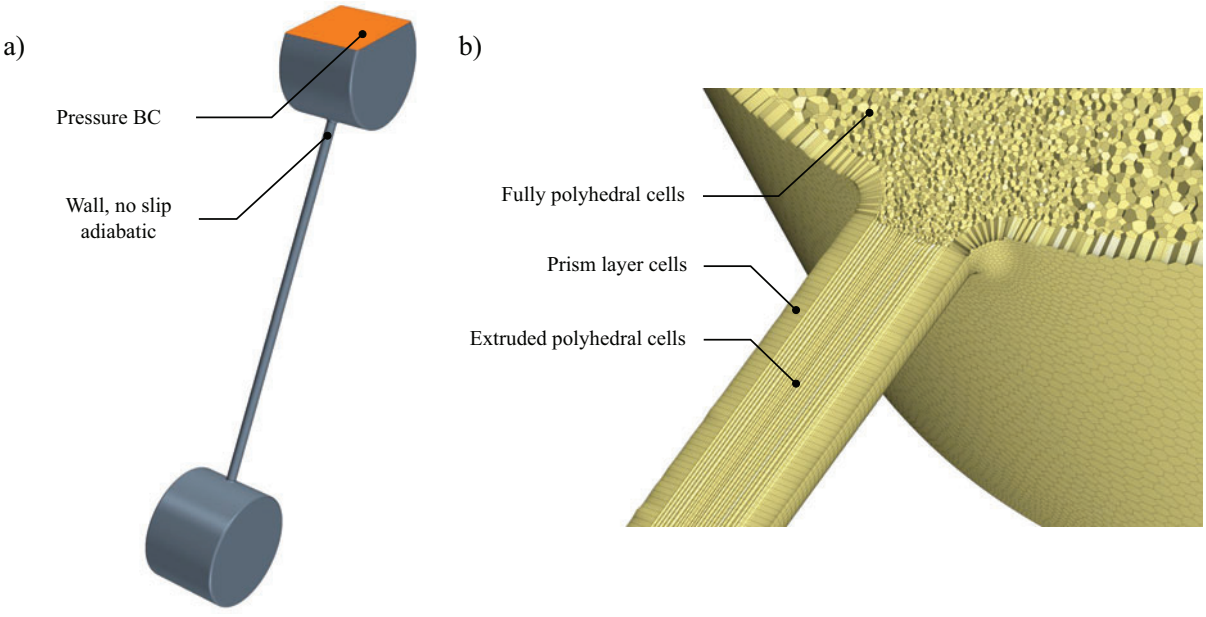

Figure 2: a) CFD model geometry and boundary conditions; b) Illustration of the mesh strategy adopted in the present study.

The temperature in the centre of the hot tank, shown in Figure 3, was monitored during the experiment and only decrease by 1% of its original value, which is mainly due to the convective heat exchange in the pipe and not the heat losses with the surroundings.
The horizontal orange surface at the top is a pressure boundary condition set to atmospheric pressure. The reason for such pressure boundary condition is to allow thermal expansion of the fluid during mixing, when the full variable density equation are used. Similarly, in the experiment itself the upper tank is not perfectly full and there is a free surface allowing for thermal expansion.
All the simulations presented below were carried out using variable tabulated fluid properties based on the IAPWS-IF97 data and the full variable density Navier-Stokes equation to ensure maximum fidelity when comparing with the experiments. However, an a-posteriori comparison between two uRANS comparison using the Boussinesq approximation and the IAPWS tabulated fluid properties showed that the predictions obtained with the Boussinesq model were only fractionally different, which would be quite satisfactory from an engineering point of view.

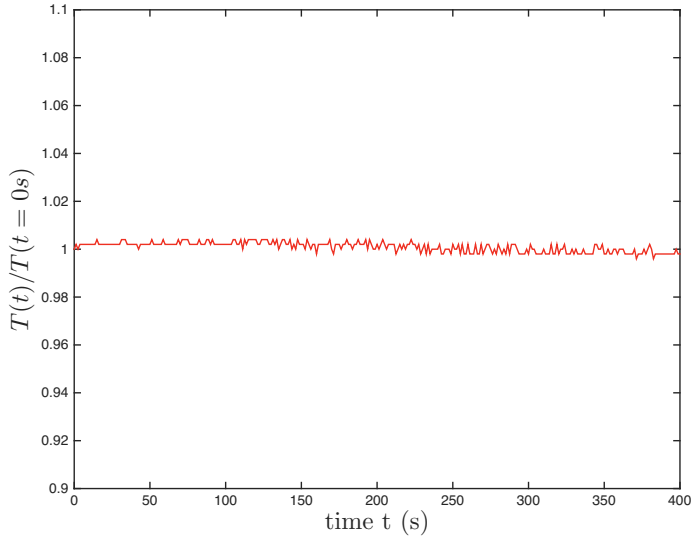

Figure 3: Measured time evolution of the temperature in the centre of the hot tank for the duration of the experiment.

3.2. Meshing Strategy

The mesh used in the present work is an unstructured polyhedral one together with prism layer cells in the vicinity of the wall in order to capture the sharp gradient in the boundary layers. The wall y^+ values for all simulations were chosen below 1 and only low-y^+ wall treatment was used in the turbulence models. Additionally, to obtain a higher quality mesh in the area of interest (the pipe cross section) extruded polyhedral cells were used as illustrated in Figure 2b. Details of the meshes used for the uRANS simulation and LES simulations are summarized in Table III. A mesh sensitivity analysis was carried out for both LES and uRANS and the solution obtained on the meshes used herein were found to be grid independent. This study is not shown here for conciseness.

Table III: Details about grid refinement

Quantity	uRANS reference mesh	LES reference mesh
Mesh base size (m)	0.1	0.1
Number of prism layers	15	20
Prism layer thickness	0.007	0.007
Prism layer expansion ratio	1.1	1.1
Minimum surface size (m)	0.002	0.001
Target surface size (m)	0.01	0.005
Number of extruded layer (pipe)	400	800
Total number of cells	1778096	5467130

3.3. Turbulence Models

Four different turbulence models were tested in the present study:

- Standard k-ε with low-Re formulation from Lien et al. [9]
- Standard k-ε with a two layer formulation near the wall from Wolfstein [10]
- Standard k-ε with a two layer formulation near the wall from Xu et al. [11]
- SST k-ω from Menter [12]

One of the aims of the present paper is to bring more generality to the observations made in our first study [6] that was based on only one flow configuration (15deg tilt angle with an Atwood number of 10^{-2}). Hence, the models selected here are only those that gave the best and worst results in the previous study where it was found that both the low-Re k-ε model and two-layer formulation from Xu et al. gave very reasonable results whereas the other two models were found to over predict the axial velocity by more than a 100% of the measured experimental value.

3.4. LES Methodology

As mentioned earlier, the mean axial velocity determines the rate of heat removal in the pipe, and hence is the most important quantity sought in a nuclear engineering context. In the present study, since only temperature is measured experimentally, the purpose of the LES simulation is to provide an accurate benchmark for the mean velocity field that can later be compared with uRANS simulations. The earlier analysis based on the experimental work of Znaien et al. [4] showed that LES can reproduce measured velocities very accurately and therefore we can expect that the LES prediction presented herein will also be accurate. Based on earlier comparison of different subgrid scale models, the dynamic formulation of the Smagorinsky [13] eddy viscosity subgrid scale model proposed by Germano [14] and improved by Lilly [15] was used.

As regards the numerical discretization for the LES, second order central difference was used. For the temporal discretization two-step implicit backward differencing was used and the maximum Courant number was kept below 0.5 with an average value around 0.3. The SIMPLE algorithm [16] was used for the pressure/velocity coupling.

3.5. Averaging Procedure

The direct comparison of the transient development of the flow is difficult since turbulence embodies a random component. uRANS simulations are based on ensemble averaged Navier-Stokes equations so for accurate comparison of the flow development one would need ensemble averaged experimental measurement and ensemble averaged LES results. This could in principle be obtained by averaging a large number of realisations of the experiment. The same could be done by running many times the LES simulation. These could then be compared with the time evolution of quantities from uRANS simulation. However this is obviously impractical. An example illustrating the difficulty to directly compare temperature evolution for experiment, LES and uRANS is shown as an example in Figure 4. Fortunately, the design of the rig was made such that the flow in the pipe section develops into a quasi-statistically steady state once the mixing front reaches each end of the tube and creates a buoyant plume in each tank. This is extremely useful for obtaining mean (i.e. averaged) quantities from the LES simulation that can be directly compared with the uRANS simulations. Time averaging can therefore be carried out to obtain the first and second statistical moments of turbulence. Looking at the evolution of the experimental measurement and later at the LES flow development, it was found that after 250s the flow in the pipe reached that state.

The experimental and numerical work of Znaien et al. [4] showed that for this particular type of flow, the mean axial velocity profile is independent of the position in the z direction in the central section of the pipe (to avoid end effects) and that the mean cross sectional density (hence the temperature) distribution is self similar in the z direction. These properties allow complementing the time averaging by spatial averaging, which considerably speeds up the convergence of the turbulent statistical moments determination. Spatial averaging in the z direction was carried out between z = -0.5m and z = 0.5m. It was found that after 150s of time and spatial averaging, the first and second order moments reached convergence. The averaging carried out for each quantity φ herein is denoted by <> and can be mathematically written as follows:

$$\left\langle \varphi\left(x,y,z,t\right)\right\rangle = \left\langle \varphi\left(x,y\right)\right\rangle = \frac{1}{1}\times\frac{1}{150}\times\int_{z=-0.5}^{z=0.5}\int_{t=250}^{t=400}\varphi\left(x,y,z,t\right)dt\,dz \tag{1}$$

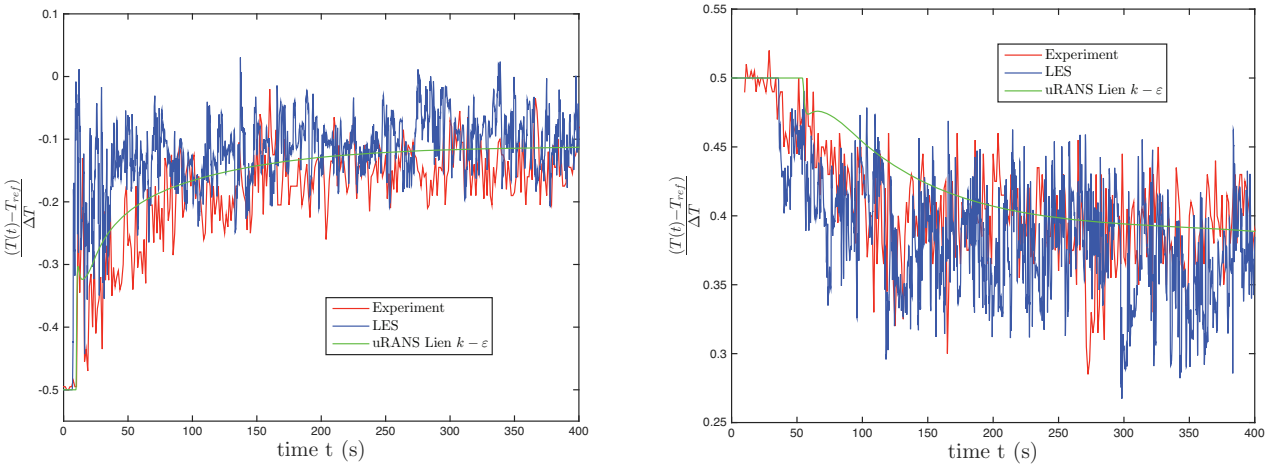

Figure 4: Time development of the temperature recorded TC-2 (left) and TC-7 (right) for the experiment, LES and uRANS simulation.

4. RESULTS

4.1. Comparison with Experimental Measurements

The present paper does not discuss the initial development of the flow as it was found to be dependent on the ball valve opening time, which was not recorded in the present set of experiments. The latter explains the difference in behaviour between CFD and experiment in the first 100s as shown in Figure 4. For the sake of clarity, all the simulations in the present paper were run as transient simulations but only the developed part of the flow was considered for validation.

Since we are not studying the initial transient development of the flow shown for illustration in Figure 5, but only the behaviour of the flow in its statistical steady state, the recording of each thermocouple is also averaged in time between 250s and 400s after the beginning of the experiment and the opening of the ball valve. The experiments were carried out three times to reduce uncertainties and the average of the three sets is used for the comparison presented below. In each simulation probes are placed at the thermocouple positions and the temperature is recorded in time, averaged and compared with the experimental results. Table IV summarises the actual averaged temperature at each location for the experiment, LES and uRANS simulations. Table V gives the relative discrepancy calculated by equation (2) between the experiment and the CFD simulation for LES and each turbulence model. The comparison between experiment and LES shows very good agreement with relative differences ranging from 0 to les than 5%. The small discrepancies observed could be explained by several factors: i) the intrusiveness of the thermocouples into the flow; ii) the possible imprecision in determining the thermocouple locations; iii) the inaccuracy of the thermocouples and/or the LES calculation.

$$D_{\text{wrt Exp}}(\%) = \frac{T_{Exp} - T_{CFD}}{\Delta T} \times 100 \tag{2}$$

Table VI finally compares the LES results with other uRANS models at each probe location by calculating the relative difference using equation (3) below.

$$D_{\text{wrt LES}}(\%) = \frac{T_{LES} - T_{uRANS}}{\Delta T} \times 100 \tag{3}$$

A very good agreement is observed between LES and other uRANS models with discrepancies below 5% at the specific probes positions, which are all in the bulk of the flow. From this comparison of the temperature obtained at the different probe location, no specific turbulence model performs better than the others. However, it will be seen in the next section that the near wall region is where major discrepancies in the prediction of the different turbulence model arise.

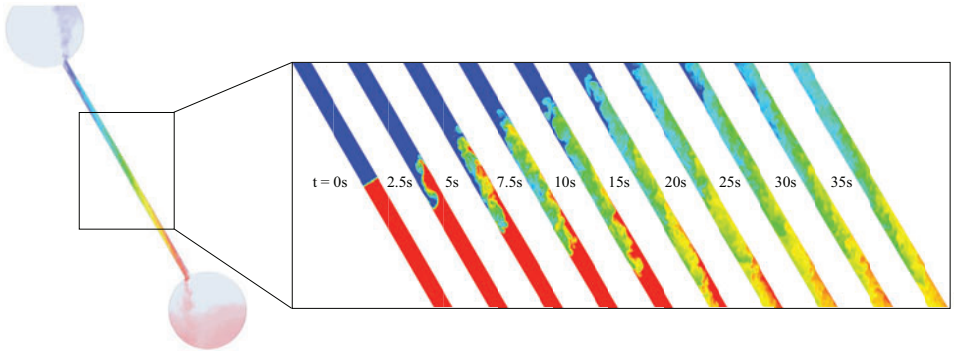

Figure 5: Illustration of the initial transient development of the flow toward a statistically steady state. These results were obtained from the LES simulation. Red and blue respectively represent hot and cold water.

Table IV: Experimental and CFD averaged temperature for each thermocouple location

Thermocouple	Experiment	LES	Low-Re k-ε (Lien)	k-ε two- layer (Wolfstein)	k-ε two-layer (Xu et al.)	SST k-ω (Menter)
TC1 (K)	311.8301	311.6175	311.2557	312.5693	311.5493	312.9646
TC2 (K)	310.6015667	310.8501	310.6623	311.593	310.9749	311.5704
TC3 (K)	316.6371667	316.9841	316.9211	317.5338	317.3093	317.9264
TC4 (K)	315.2345333	316.1625	316.1134	316.3465	316.5385	316.125
TC5 (K)	321.3611667	320.4149	320.8141	320.9049	321.0561	321.2651
TC6 (K)	319.7820333	319.3309	319.922	319.5888	320.1926	319.302
TC7 (K)	325.9082667	325.4047	326.0605	325.6922	326.1355	325.4741
TC8 (K)	324.2648	324.2491	325.1844	324.256	325.2337	323.5396

Table V: Discrepancy between CFD results for each model and experiments

Thermocouple	LES	Low-Re k-ε (Lien)	k-ε two- layer (Wolfstein)	k-ε two-layer (Xu et al.)	SST k-ω (Menter)
TC1 (%)	1.06	2.87	-3.70	1.40	-5.67
TC2 (%)	-1.24	-0.30	-4.96	-1.87	-4.84
TC3 (%)	-1.73	-1.42	-4.48	-3.36	-6.45
TC4 (%)	-4.64	-4.39	-5.56	-6.52	-4.45
TC5 (%)	4.73	2.74	2.28	1.53	0.48
TC6 (%)	2.26	-0.70	0.97	-2.05	2.40
TC7 (%)	2.52	-0.76	1.08	-1.14	2.17
TC8 (%)	0.08	-4.60	0.04	-4.84	3.63

Table VI: Discrepancy between uRANS turbulence models and LES

Thermocouple	Low-Re k-ε (Lien)	k-ε two- layer (Wolfstein)	k-ε two-layer (Xu et al.)	SST k-ω (Menter)
TC1 (%)	1.809	-4.759	0.341	-6.7355
TC2 (%)	0.939	-3.7145	-0.624	-3.6015
TC3 (%)	0.315	-2.7485	-1.626	-4.7115
TC4 (%)	0.2455	-0.92	-1.88	0.1875
TC5 (%)	-1.996	-2.45	-3.206	-4.251
TC6 (%)	-2.9555	-1.2895	-4.3085	0.1445
TC7 (%)	-3.279	-1.4375	-3.654	-0.347
TC8 (%)	-4.6765	-0.0345	-4.923	3.5475

4.2. Comparison of uRANS Turbulence Models Prediction Against LES

From this point, LES is considered to be the reference point for the analysis of the behaviour of the different uRANS turbulence models. Comparison of the thermal stratification along the axis of the pipe presented in Figure 6 shows that all models give very close prediction when compared with LES. This is directly in line with the observations made in the previous section when comparing with the thermocouple measurements. This is due to the fact that the thermocouples are inserted quite far into the pipe and close to the axis.

However, the comparison of the density distribution in the XY cross section of the pipe as illustrated in Figure 7 shows that there are very large discrepancies in the vicinity of the wall for the SST and two-layer model of Wolfstein [10]. On the other hand the other two uRANS turbulence models show a much better agreement with the LES. A more quantitative comparison of the temperature distribution is presented in Figure 8, which shows the mean temperature variation along the X direction for each turbulence model.

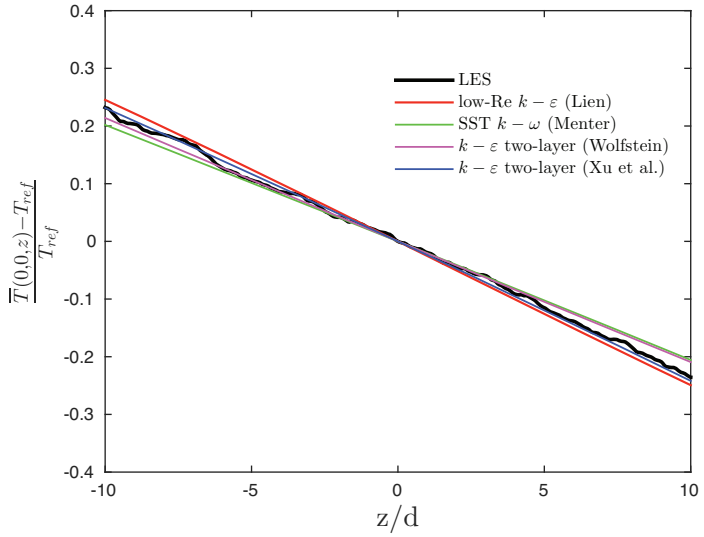

Figure 6: Comparison of the thermal stratification along the pipe axis for each turbulence model

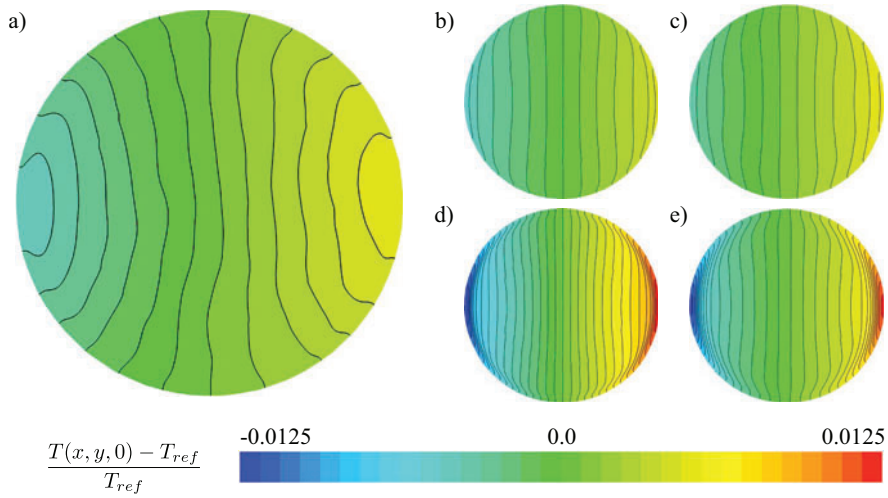

Figure 7: Comparison of the mean temperature distribution in the pipe cross section (z = 0) for LES and each uRANS model: a) LES; b) low-Re k-ε; c) two-layer Xu et al.; d) SST; e) two-layer Wolfstein

Because of the two-way coupling between the momentum and energy equation, such discrepancies in cross-sectional temperature distribution (and therefore in density) directly affect the axial velocity distribution. Indeed, the additional driving force arising from the very sharp local density gradient near the wall (obtained with the SST k-ω and two-layer models) yields a large over-prediction (more than 100% of the LES result) in the mean axial velocity as illustrated in Figure 9 and Figure 10. This can also be seen in Figure 12 where for the SST k-ω and two-layer model from Wolfstein the buoyant plumes in the tanks are much more visible than in the LES case, showing that the exchange between the two tanks occur much faster.

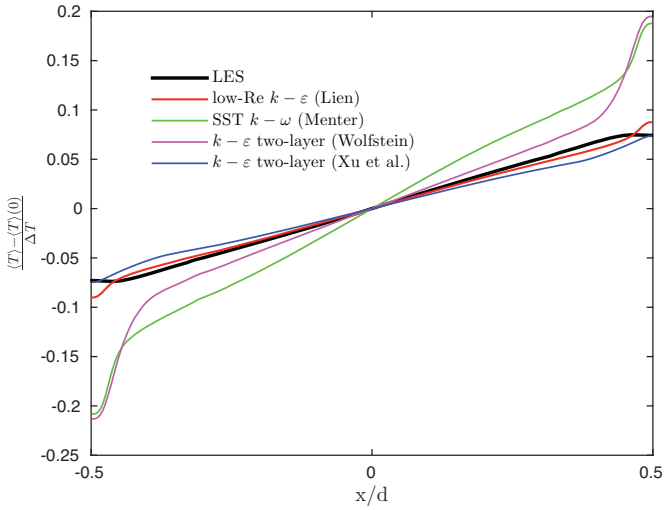

Figure 8: Comparison of the mean temperature along the X direction for each turbulence model

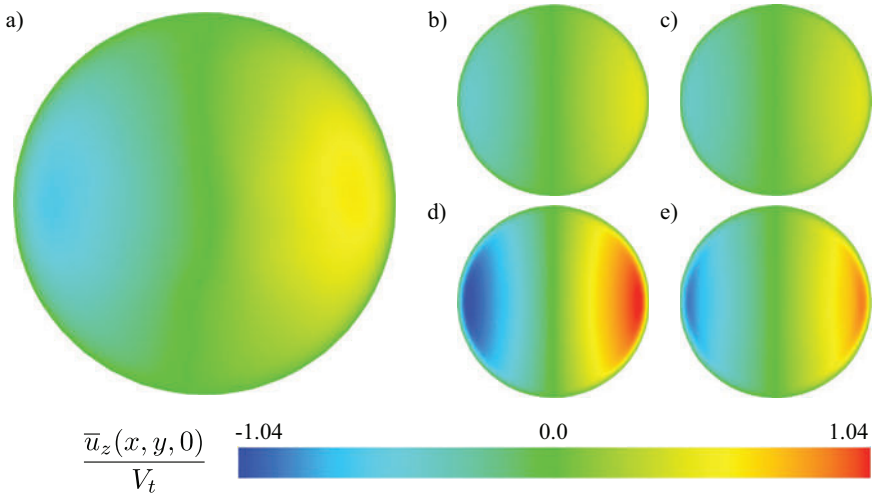

Figure 9: Comparison of the mean axial velocity distribution in the pipe cross section (z = 0) for LES and each uRANS model: a) LES; b) low-Re k-ε; c) two-layer Xu et al.; d) SST; e) two-layer Wolfstein

These results are perfectly in line with observation made in [6] using the experimental data from Znaien et al. [4], where the pipe was in a more vertical position than with the present case and had Atwood number twice as large. The predictions obtained with the other two models (low-Re k-ε and two-layer from Xu et al.) are much better when compared to the LES velocity profile. However, they underpredict the mean axial velocity by approximately 20% when comparing the local extremum. It is worth noting

that this under-prediction was not found in the previous study [6]. This might suggest that the transverse gravity component plays an important role and that further testing in more horizontal configurations needs to be carried out.

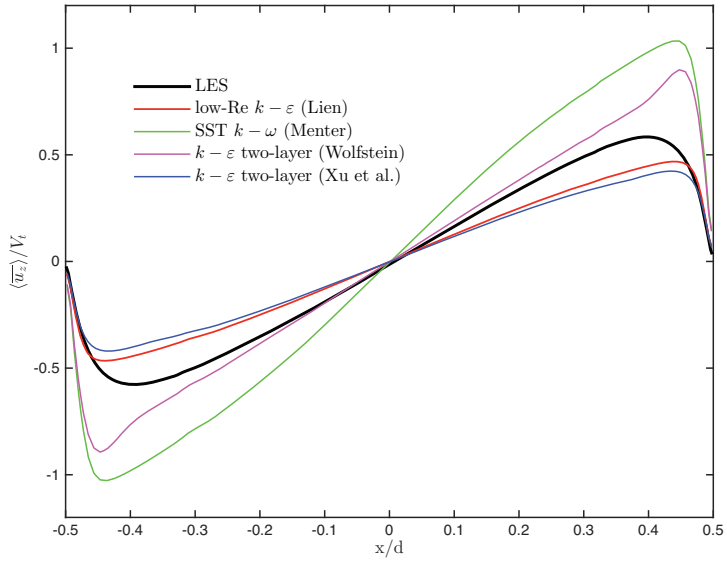

Figure 10: Comparison of the mean axial velocity prediction along the X direction for each turbulence model

As regards the comparison of turbulent kinetic energy profile shown in Figure 11, the results are directly related to the mean axial velocity prediction. In the case where the velocity is overpredicted, the turbulent kinetic energy is also over-predicted and when the axial velocity is under-predicted, the mean turbulent kinetic energy is also under-predicted.

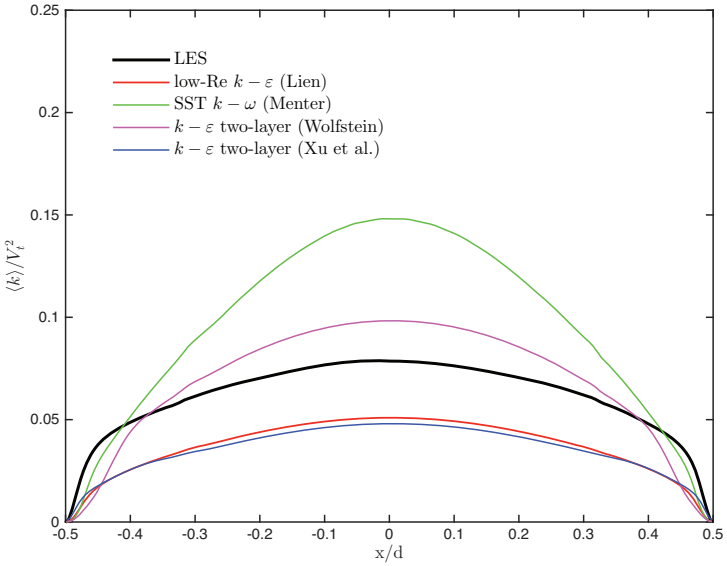

Figure 11: Comparison of the mean turbulent kinetic energy distribution for each turbulence model along the X direction

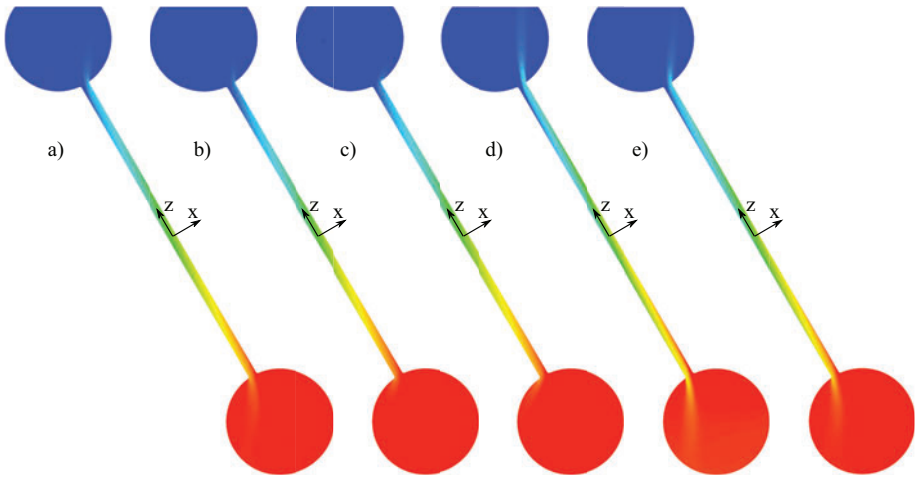

Figure 12: Comparison of the time-averaged temperature distribution in the XZ section (y = 0) for each turbulence model: a) LES; b) low-Re k-ε; c) two-layer Xu et al.; d) SST; e) two-layer Wolfstein. Red and blue respectively represent the hot and cold water.

5. CONCLUSIONS

In the present paper, single-phase counter-current flow was studied both experimentally and numerically in a pipe tilted at a 30deg angle from vertical and an initial temperature difference of 20K. A good agreement between LES and experimental measurement was found.

Comparison of four two-equation eddy viscosity based turbulence models with the highly resolved LES showed that the wall treatment is the most important to obtain good prediction of the axial velocity. The SST k-ω turbulence model as well as the k-ε two-layer model from Wolfstein were both found to over-predict the axial velocity by a factor of two. On the other hand the low-Re k-ε and two-layer approach from Xu et al. showed a better prediction of the cross-sectional density distribution, which therefore lead to a much better prediction of the mean axial velocity. These results are in line with the previous study obtain in a more vertical configuration and with a different Atwood number, which tends to suggest that the choice of appropriate turbulence model to simulate single phase buoyancy induced counter-current flow has some generality.

6. NOMENCLATURE

u_i		Instantaneous velocity component in the ith direction
$\overline{u}_i$		Ensemble averaged (uRANS) or filtered (LES) velocity
p		Pressure
T		Temperature of the fluid
T_c		Temperature of the cold fluid
T_h		Temperature of the hot fluid
ρ_c		Density of the cold fluid
ρ_h		Density of the hot fluid
At	$\frac{\rho_c - \rho_h}{\rho_c + \rho_h}$	Atwood number
d		Pipe diameter

g		Gravitational acceleration
V_t	$\sqrt{\mathrm{At}gd}$	Characteristic velocity
LES		Large Eddy Simulation
uRANS		Unsteady Reynolds Averaged Navier Stokes

7. ACKNOWLEDGMENTS

The authors would like to acknowledge Rolls-Royce for funding the research, Imperial College for the HPC resources made available and CD-adapco for providing the package STAR-CCM+ used herein.

8. REFERENCES

1. Reyes Jr, J.N., *Flow Stagnation under Single and Two-Phase Natural Circulation Conditions in the APEX-CE Test Facility.* Science and Technology of Nuclear Installations, 2008. **2008**.
2. Séon, T., et al., *Buoyancy driven miscible front dynamics in tilted tubes.* Physics of fluids, 2005. **17**.
3. Seon, T., et al., *Laser-induced fluorescence measurements of buoyancy driven mixing in tilted tubes.* Physics of Fluids, 2006. **18**(4): p. 041701-4.
4. Znaien, J., et al., *Experimental and numerical investigations of flow structure and momentum transport in a turbulent buoyancy-driven flow inside a tilted tube.* Physics of Fluids, 2009. **21**(11): p. 115102.
5. Znaien, J., F. Moisy, and J.-P. Hulin, *Mélange turbulent de fluides sous l'effet de la gravité dans un tube incliné*, in *19ème congrès Français de Mécanique*. 2009: Marseille.
6. Sebilleau, F., R.I. Issa, and S.P. Walker, *Analysis of the turbulence modelling approaches to model buoyancy driven counter-current flow in a tilted tube.* under review in Flow, Turbulence and Combustion, 2015.
7. CD-ADAPCO, *Star-CCM+ user guide v9.04.011*. 2014.
8. Sebilleau, F., et al. *CFD analysis of single phase counter-current buoyancy driven flows and its applications to passive reactor design*. in *ICONE22*. 2014. Prague, Czech Replublic.
9. Lien, F.S., W.L. Chen, and M.A. Leschziner, *Low-Reynolds-Number eddy-viscosity modelling based on non-linear stress-strain/vorticity relations*. Engineering Turbulence Modelling and Experiments 3, ed. W. Rodi and G. Bergeles. 1996. 91-100.
10. Wolfshtein, M., *The velocity and temperature distribution in one-dimensional flow with turbulence augmentation and pressure gradient.* International Journal of Heat and Mass Transfer, 1969. **12**(3): p. 301-318.
11. Xu, W., Q. Chen, and F.T.M. Nieuwstadt, *A new turbulence model for near wall natural convection.* International Journal of heat and mass transfer, 1998. **41**: p. 3161-3176.
12. Menter, F.R., *Two-equation eddy-viscosity turbulence models for engineering applications.* AIAA Journal, 1994. **32**(8): p. 1598-1605.
13. Smagorinsky, J., *General circulation experiments with the primitive equations.* Monthly Weather Review, 1963. **91**(3): p. 99-164.
14. Germano, M., et al., *A dynamic subgrid-scale eddy viscosity model.* Physics of Fluids A: Fluid Dynamics, 1991. **3**(7): p. 1760-1765.
15. Lilly, D.K., *A proposed modification of the Germano subgrid-scale closure method.* Physics of Fluids A: Fluid Dynamics, 1992. **4**(3): p. 633.
16. Patankar, S.V. and D.B. Spalding, *A calculation procedure for heat, mass and momentum transfer in three-dimensional parabolic flows.* International Journal of Heat and Mass Transfer, 1972. **15**(10): p. 1787-1806.